International Geology Review
Vol. 53, Nos. 5–6, April–May 2011, 499–525

Taylor & Francis
Taylor & Francis Group

Geochemical and zircon U–Pb study of the Huangmeijian A-type granite: implications for geological evolution of the Lower Yangtze River belt

He Li[a,b], Hong Zhang[a,b], Ming-Xing Ling[a,b], Fang-Yue Wang[a,b], Xing Ding[a], Ji-Bin Zhou[a], Xiao-Yong Yang[c], Xiang-Lin Tu[a] and Weidong Sun[a,c]*

[a]*CAS Key Laboratory of Isotope Geochronology and Geochemistry, Guangzhou Institute of Geochemistry, The Chinese Academy of Sciences, Guangzhou, PR China;* [b]*Graduate University of the Chinese Academy of Sciences, Beijing, PR China;* [c]*School of Earth and Space Sciences, University of Science and Technology of China, Hefei, PR China*

(*Accepted 5 April 2010*)

The Early Cretaceous Huangmeijian Pluton is an A-type granite located on the northern bank of the Lower Yangtze River in Anhui Province, east-central China. It intruded the SE edge of the Early Cretaceous Luzong volcanic basin. The moderate- to coarse-grained granite is mainly composed of alkali feldspar, plagioclase, and quartz and has a typical A-type geochemical signature. LA-ICP-MS zircon dating yielded a weighted mean $^{206}Pb/^{238}U$ age of 127.1 ± 1.4 Ma, similar to other A-type granites in the Lower Yangtze River belt, indicating an Early Cretaceous extensional environment. Temperatures calculated using the Ti-in-zircon thermometer suggest that the magma formed under high-temperature conditions (720–880°C). The low calculated Ce(IV)/Ce(III) ratio based on zircon rare earth element patterns indicates low oxygen fugacity for this A-type magma. Previous studies suggested that eastern China was an active plate margin related to the Early Cretaceous subduction of the Pacific and Izanagi plates. The ridge between these two plates probably passed under the Lower Yangtze River belt, forming A-type granites and adakites. The Huangmeijian Pluton is roughly the same age within error but is marginally older than the Baijuhuajian A-type granite in the eastern part of the Lower Yangtze River belt. A-type granite genesis in the Lower Yangtze River belt only lasted for 2–3 million years and slightly predates the transition from regional extension to compression. All these can be plausibly interpreted by the ridge subduction model, that is, A-type granites formed because of mantle upwelling through the slab window during subduction of the ridge separating the Pacific and Izanagi plates.

Keywords: A-type granitic intrusion; geochemistry; LA-ICP-MS zircon dating; Huangmeijian Pluton; Luzong volcanic basin; east-central China

Introduction

The Lower Yangtze River belt (LYRB), which ranges from Wuhan in Hubei province in the west to Zhenjiang in Jiangsu province in the east, is an important metallogenic belt in eastern China (Chang *et al.* 1991; Zhai *et al.* 1992, 1996; Pan and Dong 1999; Xing 1999; Deng *et al.* 2002). Most of the deposits in the LYRB formed during the Early Cretaceous

*Corresponding author. Email: weidongsun@gig.ac.cn

ISSN 0020-6814 print/ISSN 1938-2839 online

DOI: 10.1080/00206814.2010.496202
http://www.informaworld.com

period (140 ± 5 Ma) (Sun *et al.* 2003; Mao *et al.* 2006; Yang *et al.* 2007), and they are closely associated with adakites of the same age (Zhang *et al.* 2001a, b; Wang *et al.* 2004a, b, 2006, 2007). Much attention has been focused on the geological evolution of this region (e.g. Xing and Xu 1994, 1995; Chen and Jahn 1998; Zhou and Li 2000; Chen *et al.* 2001; Sun *et al.* 2007; Fan *et al.* 2008; Yuan *et al.* 2008; Xie *et al.* 2008; Zhou *et al.* 2008a, b; Ling *et al.* 2009; Xie *et al.* 2009; Yang *et al.* 2011). In addition to adakite, there are a large number of Cretaceous A-type granites along both banks of the LYRB (Zhang *et al.* 1988; Xing and Xu 1994; Fan *et al.* 2008; Wong *et al.* 2009). The age and formation of A-type granite is important for understanding the geological evolution of the LYRB.

The genesis of A-type granites in the LYRB remains controversial. A-type granite is anhydrous, alkaline, and anorogenic, which generally indicates formation in an extensional environment (Loiselle and Wones 1979; Eby 1990, 1992; Bonin 2007). The extensional environment in the LYRB was proposed to be either back-arc and post-collision extension settings (Du *et al.* 2007; Cao *et al.* 2008) or intracontinental shearing effect associated with mantle upwelling (Fan *et al.* 2008). Alternatively, it has been attributed to slab rollback of subducting Pacific plate (e.g. Wong *et al.* 2009) or a ridge subduction (Ling *et al.* 2009) based on the drifting history of the Pacific plate (Sun *et al.* 2007). The ridge subduction model implies that A-type granites in the LYRB would be progressively younger from west to east. Previously published dating results have not observed this (e.g. Zheng *et al* 1995; Fan *et al*. 2008; Wong *et al.* 2009).

In this contribution, we analysed the geochemistry and zircon ages of the Huangmeijian A-type granite on the northern bank of the LYRB to gain a better understanding of the genesis of A-type granite in the LYRB and firmer constraints on the geological evolution of the LYRB.

Geological background

The LYRB is situated in the northern margin of the Yangtze block in central eastern China (Figure 1A). The northern and northwestern boundaries of the region are the Xiangfan-Guangji and the Tancheng-Lujiang faults, which separate the Dabie orogenic belt in the north and the Yangtze block in the south, respectively. The southern boundary is the Jiangshan-Shaoxing fault that separates the Yangtze block from the Cathaysia block (Figure 1A). Late Mesozoic igneous rocks are widely outcropped in the LYRB. These igneous rocks intrude into Neoproterozoic low-grade metamorphic rocks and Palaeozoic to Triassic sedimentary strata, and are classified into three associations: Na-rich alkaline mafic, K-enriched, and high potassium calc-alkaline associations (Chang *et al.* 1991). According to tectonic, magmatic, and metallogenic characteristics, the LYRB can be divided into three associated belts: inner belt, north outer belt, and south outer belt (Xing and Xu 1995; Xing 1999). The inner belt, distributed along both banks of the Lower Yangtze River, has intense mineralization of Cu, Fe, S, and Au (Pan and Dong 1999; Xie *et al*. 2009; Huang *et al*. 2011; Yang and Lee 2011; Yuan *et al*. 2011; Sun *et al.* 2010, 2011), which are closely associated with adakites (Wang *et al.* 2004a, b, 2006, 2007; Ling *et al.* 2009). The north outer belt has Cu deposits, such as the Shaxi Cu deposit (Yang *et al*. 2007, 2011; Yu *et al.* 2008). The south outer belt contains mainly porphyry-type Mo, Cu, and Pb–Zn deposits (Xing 1999; Mao *et al.* 2006). Two A-type granite belts are distributed parallely on both banks of the Lower Yangtze River (Xing and Xu 1994) (Figure 1B). The Huangmeijian granite, situated at the southeast edge of Luzong Basin in Anhui province, is one of the largest A-type granite plutons on the northern bank of the Lower Yangtze

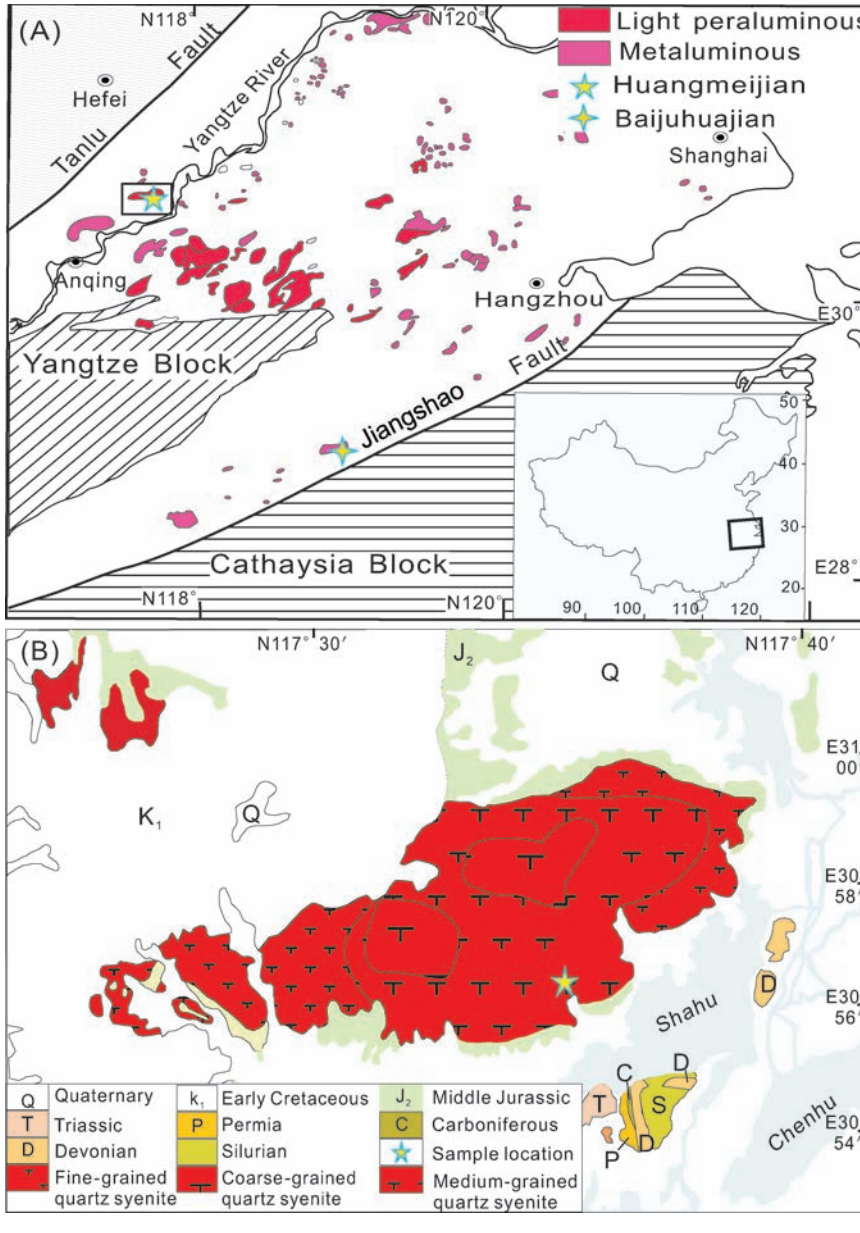

Figure 1. (A) Regional geological map of Lower Yangtze River. (B) Geological map of the Huangmeijian granite. Modified after Chen (2001).

River. It intruded in the Middle and Lower Jurassic sediment rocks in the east and in the Upper Cretaceous volcanic rocks in the west. No Jurassic volcanic rock in the Luzong Basin has been confirmed so far (Zhou *et al.* 2008b). Huangmeijian granites are faint red with moderate- to coarse-grained texture and are mainly composed of potassium feldspar (80–85%), quartz (10–15%), and plagioclase (5–10%) (Figure 2).

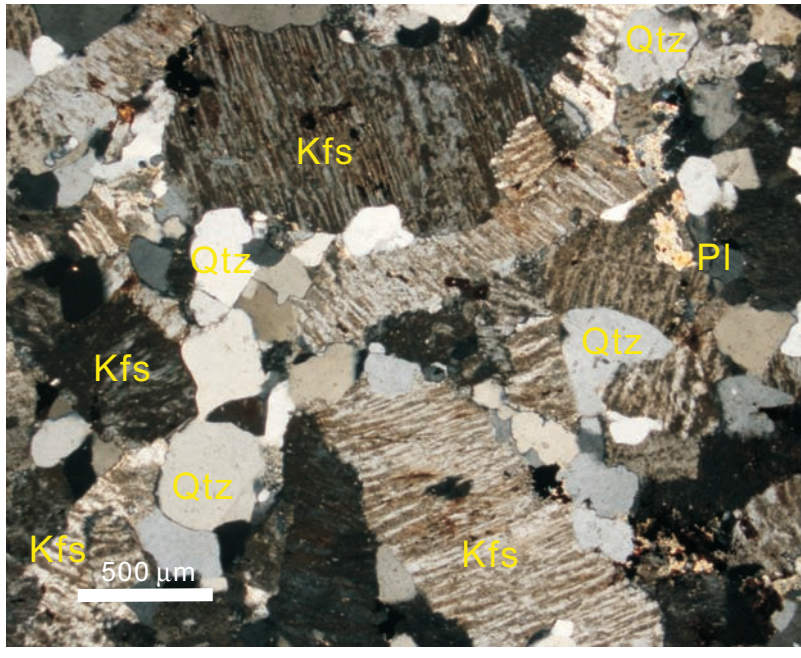

Figure 2. Photomicrographs of Huangmeijian A-type granites. The images were taken with a Nikon microscope under polarized light conditions. The scale bar for each image is 0.50 mm. Samples are mainly composed of alkali-feldspar, quartz, and plagioclase. Kfs, potassium feldspar; Pl, plagioclase; and Qtz, quartz.

Analytical methods

Whole-rock major and trace element analyses

The major and trace elements of the bulk rock samples were analysed at the Key Laboratory of Isotope Geochronology and Geochemistry, Guangzhou Institute of Geochemistry, Chinese Academy of Sciences. Whole-rock samples were first powdered in an agate mill to less than 200 mesh, and then fluxed with $Li_2B_4O_7$ to make homogeneous glass disks at 1150–1200°C using a V8C automatic fusion machine produced by the Analymate Company in China. The bulk rock major elements were analysed by X-ray fluorescence spectrometry (Rigaku 100e), with a sample/flux ratio of 1 : 8. Analytical precision for major elements was better than 1% (Ma *et al.* 2007).

For trace element analyses, samples were first digested with a mixture of HF and HNO_3 in screw top PTFE-lined stainless steel bombs at 185°C for 2 days, and insoluble residues were dissolved in HNO_3 after being heated to 145°C for 3 h using closed high-pressure bombs to ensure complete digestion. Pure RH standard solutions were used for internal calibration and GSR-1, BHVO-1, and OU-6 were used as reference materials to monitor data quality. Bulk rock trace elements were analysed using ICP-MS, with accuracies of better than 5% for most elements (Liu *et al.* 1996).

Zircon U–Pb dating and zircon trace element analyses

Zircons were separated using a conventional method, which involved powdering samples to 80 mesh, desliming in water, density separation, magnetic separation, and finally handpicking.

Zircon grains were then mounted in epoxy and polished down to nearly a half section to expose internal structures. Cathodoluminescent and optical microscopy images were taken to ensure that the least fractured, inclusion-free zones in zircon were analysed. Zircon U–Pb dating and trace elements were analysed at the Key Laboratory of Isotope Geochronology and Geochemistry, Guangzhou Institute of Geochemistry, Chinese Academy of Sciences. The LA-ICPMS system is composed of an Agilent 7500a ICP-MS coupled with a Resonetic RESOLution 50-M ArF-Excimer laser source (λ = 193 nm). Laser energy was 80 mJ and frequency was 10 Hz with ablation spot of 31 μm in diameter and 40 s ablation time. Both a double-volume sampling cell and a Squid pulse-smoothing device were used to improve data quality (Tu *et al.* 2009). Helium gas was used as the carrier gas to the ICP source. NIST610 and TEM were used as external calibration standards and ^{95}Zr as the internal standard. The calculation of isotope ratios, trace elements, and Ce anomalies were performed using software from the Research School of Earth Sciences, Australian National University; the age was calculated by Isoplot (Version 3.23).

Results

Whole-rock major and trace elements

Ten samples were analysed for major and trace element compositions. The Huangmeijian granite is characterized by high SiO_2 (64.3–74.1 wt.%), Al_2O_3 (13.4–17.4 wt.%), $Fe_2O_3^T$ (2.12–3.62 wt.%), Na_2O (4.30–5.56 wt.%), K_2O (4.85–6.99 wt.%) contents, and lower TiO_2 (0.15–0.53 wt.%), MgO (0.02–1.13 wt.%), CaO (0.12–0.53 wt.%), and P_2O_5 (0.01–0.10 wt.%) contents in comparison to other rocks of similar age in the LYRB (Table 1). According to the Q'-ANOR diagram of Streckeisen and Le Maitre (Streckeisen and Le Maitre 1979) (Figure 3A), the samples are classified as alkali-feldspar quartz-syenite. They are metaluminous or metaluminous-peraluminous rocks with A/CNK [molar $Al_2O_3/(CaO + Na_2O + K_2O)$] values of 0.96–1.12 (Figure 3B). In Hacker diagrams, TiO_2 and $Fe_2O_3^T$ decrease with increasing SiO_2, indicating fractional crystallization of Ti–Fe oxide (Figure 4).

Most of the samples have low Sr (7.20–27.4 ppm) and high Nb (71.8–118 ppm) and Rb (322–572 ppm) concentrations; they also have high rare earth elements (REEs), with total REE concentrations of 210–667 ppm. A chondrite-normalized REE diagram shows that the Huangmeijian samples are LREE enriched (La_N/Yb_N = 7.19–15.7) with flat heave REE and negative Eu anomalies (Eu/Eu* = 0.09–0.87), which indicates the removal of plagioclase by fractional crystallization (Figure 5). The decrease in Sr and Ba and slight increase in Rb with increasing SiO_2 may also be due to plagioclase fractionation. Negative anomalies in Ba, Sr, and Eu, as shown in the primitive mantle-normalized trace element diagram (Figure 6), suggest fractional crystallization of feldspar. In contrast, Nb, Ta, Zr, and Hf are not depleted, implying little contribution of crustal- or subduction-related material in the magma source. The depletion of Ti coupled with high Nb and Ta concentrations suggests crystallization of ilmenite, with little influence of rutile or titanite. Ilmenite, rutile, and titanite are the three popular Ti minerals (Liou *et al.* 1998). Rutile and titanite usually have high concentrations of Nb and Ta (Manning and Bohlen 1991; McDonough 1991; Green 1995; Rudnick *et al.* 2000; Foley *et al.* 2002; Xiong *et al.* 2005; Xiao *et al.* 2006; Ding *et al.* 2009; Liang *et al.* 2009). In contrast, ilmenite usually has much lower Nb and Ta (Ding *et al.* 2009). Thus, crystallization of ilmenite takes Ti out of the magma, leading to depletion of Ti in the granite without significant decrease of Nb and Ta.

Table 1. Major element data for the Huangmeijian granite and the Baijuhuajian granite (wt.%).

Sample	SiO_2	TiO_2	Al_2O_3	$Fe_2O_3^T$	MnO	MgO	CaO	Na_2O	K_2O	P_2O_5	LOI	Total
08HMJ01	71.9	0.15	13.4	3.43	0.05	0.02	0.25	4.3	5.19	0.02	0.9	99.6
08HMJ02	66.9	0.43	16.3	3.16	0.09	0.04	0.28	5.6	5.98	0.05	0.76	99.6
08HMJ03	68.9	0.3	15.2	2.92	0.04	0.08	0.51	5.23	5.76	0.03	0.71	99.6
08HMJ04	67	0.4	16.3	2.82	0.09	0.11	0.48	5.56	6.1	0.04	0.85	99.7
08HMJ05	69	0.33	15	3.04	0.07	0.03	0.41	4.98	5.85	0.03	0.88	99.6
08HMJ07	69.5	0.29	15.2	2.68	0.04	0.05	0.12	4.69	6.1	0.04	0.81	99.6
08HMJ08	69.7	0.34	15.4	2.98	0.07	0.02	0.15	5.07	5.95	0.03	0.76	100.4
08HMJ09	74.1	0.16	13.5	2.12	0.02	0.03	0.08	4.05	4.85	0.01	0.87	99.7
08HMJ10	65.2	0.48	17.4	2.62	0.08	0.09	0.53	5.12	6.99	0.09	1.02	99.6
08HMJ11	64.3	0.53	17.4	3.62	0.1	0.13	0.5	4.96	6.5	0.1	1.5	99.7
HMJ12	73.1	0.15	13.2	3.25	0.05	0.22	0.65	4.31	4.95	0.04	0.58	100.4
HMJ13	61	0.68	17.9	4.22	0.05	0.83	1.93	5.38	6.96	0.2		99.6
HMJ14	65.5	0.41	18.2	2.89	0.21	0.15	0.36	6.33	5.68	0.03	0.7	100.2
HMJ15	64.3	0.56	17.6	3.24	0.14	0.38	0.58	6.45	6.32	0.08	0.45	100
HMJ16	68.5	0.35	15.6	3.10	0.09	0.23	0.35	4.98	5.99	0.17	0.57	99.8
HMJ17	67.4	0.37	15.8	3.30	0.11	0.36	0.71	5.27	6.18	0.08	0.79	100.2
HMJ18	68.1	0.36	16.2	2.89	0.07	0.29	0.48	4.76	6.4	0.06	0.8	100.4
HMJ19	64	0.4	17.9	3.48	0.08	0.19	0.59	5.72	6.09	0.14	0.84	99.4
HMJ20	60.5	0.74	18.3	5.20	0.03	0.69	2.41	4.97	6.17	0.04	1.84	100.6
HMJ21	64.3	0.55	17.1	3.79	0.08	0.36	1.12	5.3	6.67	0.17	0.54	99.8
HMJ22	64	0.71	17	2.91	0.22	1.03	2.09	5.04	6.18	0.21		99.4
L2801	73.06	0.15	13.19	3.25	0.05	0.22	0.65	4.31	4.95	0.04	0.58	100.38
06ZFR01	76.2	0.06	11.5	2.83	0.12	0.1	0.56	2.36	3.85	0	1.43	99
06ZFR02	75.2	0.13	12.4	1.89	0.03	0.11	1.01	3.04	5.03	0	0.9	99.8
06ZFR08	76.9	0.1	11.6	1.22	0.04	0.06	0.55	3.99	4.07	0	0.8	99.4
07ZFR01	76.2	0.12	11.7	1.44	0.02	0.12	0.65	3.65	4.23	0	0.77	98.9
07ZFR02	76.6	0.11	11.8	1.33	0.02	0.11	0.53	3.89	4.04	0	0.83	99.3
07ZFR03	77.3	0.11	12	1.35	0.02	0.1	0.57	3.87	3.97	0	0.67	99.9
07ZFR04	77.3	0.07	12.4	0.55	0.01	0.07	0.51	3.5	5.02	0	0.55	99.9
07ZFR05	77.1	0.1	12	1.24	0.02	0.11	0.59	3.45	4.58	0	0.72	99.9
07ZFR06	76.9	0.1	12	0.94	0.01	0.07	0.54	3.7	4.61	0	0.7	99.6
07ZFR07	77.1	0.1	11.9	1.36	0.02	0.09	0.55	3.61	4.26	0	0.77	99.7
07ZFR08	77.1	0.1	12.1	1.43	0.02	0.09	0.56	3.5	4.36	0	0.77	100
07ZFR09	76.7	0.12	11.8	1.57	0.02	0.09	0.56	3.5	4.22	0	0.9	99.4
07ZFR10	77.7	0.1	11.5	0.78	0.02	0.05	0.56	3.99	4.24	0	0.73	99.6
07ZFR11	77.3	0.09	11.5	1.14	0.04	0.06	0.56	3.69	4.29	0	0.8	99.5
07ZFR12	76.9	0.1	12	1.08	0.01	0.07	0.53	3.78	4.4	0	0.8	99.7
07ZFR13	76.6	0.1	12.2	1.09	0.01	0.07	0.54	3.64	4.53	0	0.67	99.4

Note: LOI = loss on ignition. n.d. = not detected. $Fe_2O_3^T$ = Total Fe oxides represented in form of Fe_2O_3. 08HMJ01 to 08HMJ11 samples are quartz-syenite from this article, HMJ12 and HMJ21 data are from Xing and Xu (1994), HMJ12 is fine-grained granite, HMJ13 is moderate-grained biotite-monzonite, HMJ14 is coarse-grained syenite, HMJ15 is amphibole-syenite, HMJ16 is midcourse-grained quartz-syenite, HMJ17 is fine-grained maculosus quartz-syenite, HMJ18 is fine-grained quartz-syenite, HMJ19 is orthophyre, HMJ20 is maculosus biotite-syenite, HMJ21 is biotite-quartz-syenite (Xing 1994), HMJ22 is quartz-orthophyre from Cao (2008), L2801 is quartz-syenite are from Fan (2008), 06ZFR01 to 07ZFR13 data are from Wong (2009).

Compared to Baijuhuajian A-type granite in northeastern Quzhou, western Zhejiang Province, in the northwest region of the NW-trending Jiangshan-Shaoxing fault zone (Wong *et al.* 2009), samples from Huangmeijian have lower SiO_2 and higher CaO, TiO_2, $Fe_2O_3^T$, P_2O_5, Sr, and Ba. In Hacker diagrams, samples from both rocks have a good negative linear relationship between SiO_2 and CaO, TiO_2, $Fe_2O_3^T$, P_2O_5, Sr, and Ba. In a chondrite-normalized REE diagram, Huangmeijian samples have higher light REE (LREE) and lower heavy REE (HREE) patterns, with stronger negative Eu anomaly.

Table 2. Trace element data for bulk samples from the Huangmeijian granite (ppm).

ppm	08HMJ01	08HMJ02	08HMJ03	08HMJ04	08HMJ05	08HMJ07	08HMJ08	08HMJ09	08HMJ10	08HMJ11
Sc	1.26	4.27	3.1	3.97	3.03	2.47	3.38	1.04	5.07	5.96
V	1.74	3.73	4.65	5.57	6.28	5.1	6.44	3.67	22	22.8
Cr	14.7	3.55	6.35	7.07	8.93	8.26	8.44	8.18	9.43	15.3
Mn	439	784	370	746	587	367	665	130	791	917
Co	1.94	1.32	0.97	1.33	1.26	1.16	2.17	1.34	1.79	2.31
Ni	5.67	0.43	0.89	1.88	2.74	2.4	2.27	2.73	2.96	4.02
Cu	19.6	4.5	3.92	8.09	9.79	9.54	8.69	11.11	12.9	11
Zn	47.6	39.4	27.6	45.4	40.2	34.3	62.2	25.9	41.4	87.4
Ga	27.8	26.5	26.4	25.4	27.6	26.9	27.8	25.4	22.1	21
Ge	1.76	1.74	2.02	2.55	2.76	2.65	2.74	2.6	2.03	1.87
Rb	445	416	478	335	572	544	496	322	227	218
Ba	36.2	38.4	34.2	26.2	24.4	40.6	49.8	29.3	155	181
Th	86.9	55.3	70.5	48.9	72.2	82.4	73.6	67	20.8	14.9
U	16.2	19.3	17.6	10.9	14.5	14.6	19.6	14.9	3.77	3.37
Nb	83.8	75.4	91	71.8	112	118	96.1	72.5	32.7	35
Ta	8.05	5.4	7.24	4.32	7.46	7.12	6.42	6.54	2.04	1.99
La	65.7	78.3	107	129	132	116	130	71.7	53.9	44.2
Ce	145	174	282	260	259	227	212	128	109	78.8
Pb	29.2	20.9	13.7	14.2	16.8	18.2	20.2	10.2	20.5	28.2
Pr	15.1	18.8	25.3	29.2	32	23.4	21.2	12.3	10.5	8.52
Sr	10	16.6	27.4	20	16.3	17.1	17.4	7.25	77.2	66
Nd	46.7	62.8	84.1	92.3	101.1	69.7	63.8	38.4	33.5	28.7
Zr	511	1173	776	1099	925	843	894	333	561	786
Hf	18.2	24.9	21.3	20.5	20.8	19.2	20.8	13.3	11.1	12.8
Sm	8.9	11.4	15.3	15.2	17.3	12.4	10.6	7.87	5.83	5.63
Eu	0.24	0.54	0.52	0.68	0.5	0.4	0.42	0.27	1.45	1.37
Ti	796	1971	1548	2364	2057	1781	2115	1023	3053	3326
Gd	7.62	9.08	13.1	12.4	13.5	9.42	8.57	7.14	4.51	4.65
Tb	1.33	1.48	1.97	1.9	2.24	1.63	1.46	1.44	0.71	0.77
Dy	8.07	8.57	10.9	9.9	12.6	10.1	8.82	9.25	4.07	4.46
Y	55.3	55	73.1	58.2	74.9	58.2	49.4	57.3	22.5	25.4
Ho	1.63	1.77	2.12	1.98	2.53	2.07	1.88	2.04	0.83	0.91
Er	5.28	5.49	6.56	5.7	7.52	6.22	5.81	6.24	2.45	2.71
Tm	0.89	0.9	1.03	0.89	1.16	0.95	0.98	1.01	0.39	0.43
Yb	6.55	6.53	7.56	5.92	7.73	6.68	6.88	6.67	2.7	2.96
Lu	1.05	1.08	1.19	0.96	1.2	0.98	1.08	0.97	0.43	0.47

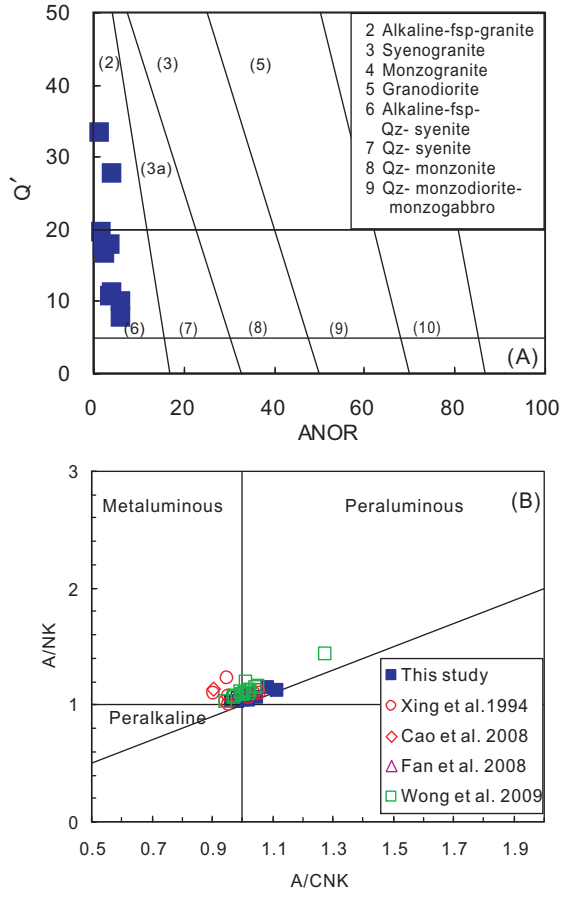

Figure 3. (A) Rock discrimination diagram for the Huangmeijian granite. Samples are classified as alkaline feldspar quartz-syenite (Streckeisen and Le Maitre 1979), where ANOR = An/ Or + An)*100; Q' = Q/(Q + Or + Ab + An). (B) A/NK versus A/CNK diagram. The Baijuhuajian granite shows a metaluminous nature. A/NK = Al/(Na + K) (molar ratio). A/CNK = Al/ (Ca + Na + K) (molar ratio).

Enrichment of the LREE indicates an enriched origin, thus the composition of Huangmeijian granite is relatively more enriched than that of Baijuhuajian granite (Table 2).

LA-ICPMS U–Pb zircon dating

The results of LA-ICP-MS analysis are listed in Table 3. Zircon CL images of sample 08HMJ02 are shown in Figure 7. Zircons from this sample are euhedral with lengths ranging from 250 to 350 μm and are characterized by a dark brown colour, which is very likely due to high U and Th concentrations. No inherited cores were observed in these zircons. U and Th concentrations varied widely (U from 370 to 2470 ppm, Th from 140 to 2170 ppm), with Th/U ratios ranging from 0.15 to 1.63, indicating a magmatic origin (Hoskin and Black 2000; Belousova *et al.* 2002; Sun *et al.* 2002). All results are concordant or nearly concordant. The data can be divided into two groups as shown in the zircon U–Pb age histogram: one group with a weighted mean $^{206}Pb/^{238}U$ age of 127.1 ± 1.4 Ma

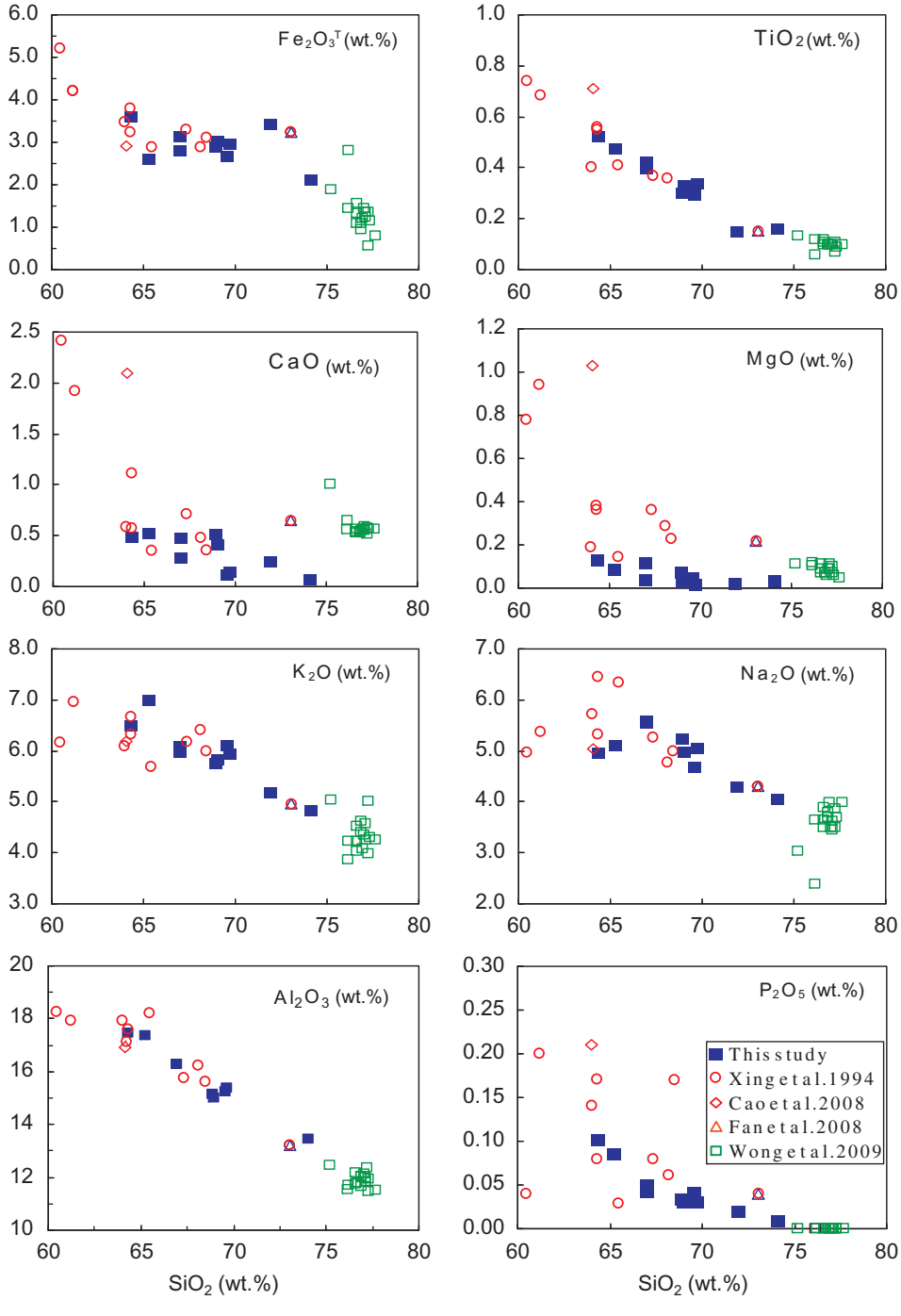

Figure 4. Hacker diagrams for the Huangmeijian granite and the Baijuhuajian granite.

(MSWD = 0.82, $n = 12$) and the other group with a weighted mean $^{206}Pb/^{238}U$ age of 142.3 ± 1.6 Ma (MSWD = 0.39, $n = 10$) (Figure 8). Given that both groups are magmatic zircon, the younger ages represent the crystallization age of the magma.

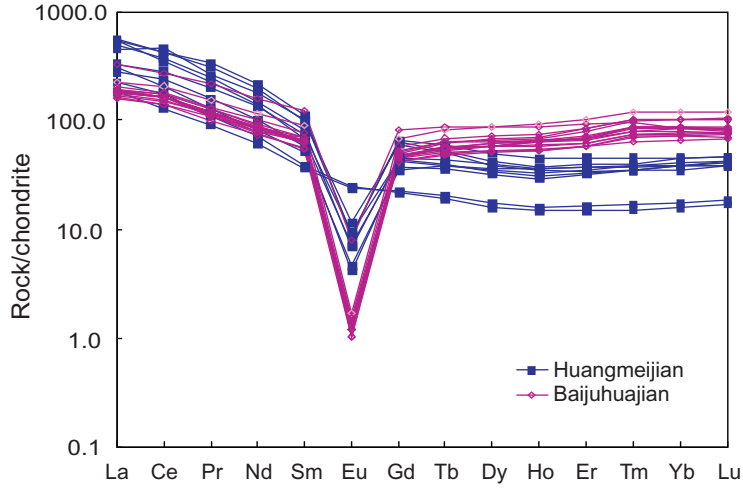

Figure 5. Chondrite-normalized REE diagram for the Huangmeijian granite and the Baijuhuajian granite.

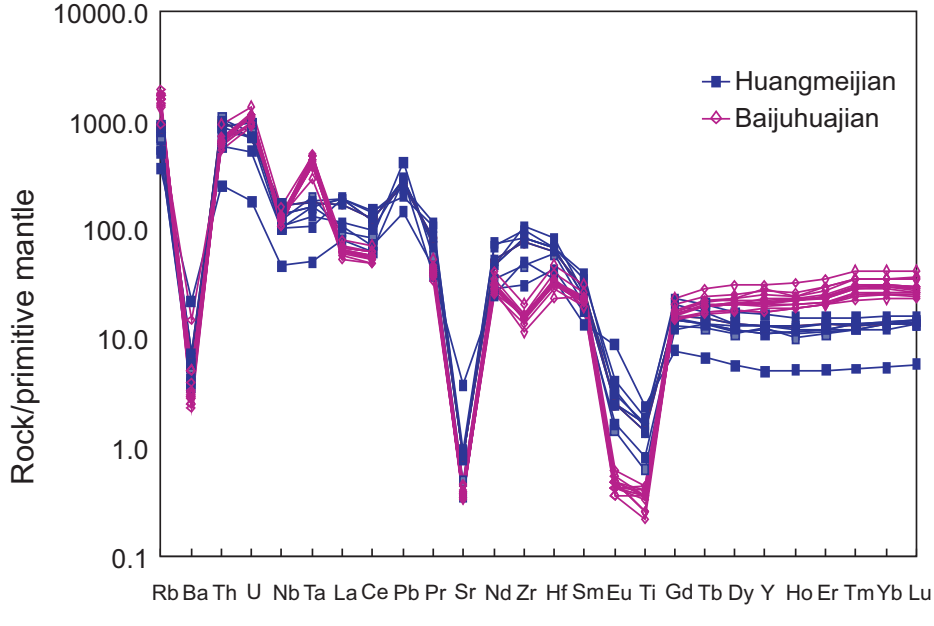

Figure 6. Primitive mantle-normalized trace element diagram for the Huangmeijian granites and the Baijuhuajian granites.

Zircon trace element patterns

The zircon chondrite-normalized REE diagram shows an Eu negative anomaly and slight Ce positive anomaly in most zircon analyses. Only a few zircon grains have a slight Ce negative anomaly (Figure 9, Table 4). The older zircons have consistent chondrite-normalized REE patterns, whereas the younger zircons have chondrite-normalized REEs

Table 3. LA-ICPMS zircon U–Pb isotope composition and age of the Huangmeijian granite.

Sample	U (ppm)	Th (ppm)	Th/U	Isotopic ratios				Age (Ma)		Ce(IV)/ Ce(III)
				$^{207}Pb/^{235}U$	2σ	$^{206}Pb/^{238}U$	2σ	$^{206}Pb/^{238}U$	2σ	
HMJ02-01	729	959	1.31	0.213	0.02	0.02	0.00047	126	2.65	6.19
HMJ02-02	1315	1777	1.35	0.136	0.02	0.02	0.00029	128	1.58	3.82
HMJ02-03	760	834	1.1	0.153	0.02	0.02	0.00039	123	2.38	4.04
HMJ02-04	1957	301	0.15	0.143	0.01	0.02	0.00025	128	1.55	5.09
HMJ02-05	1327	2169	1.63	0.244	0.03	0.021	0.00057	130	3.06	2.3
HMJ02-06	1476	743	0.5	0.153	0.01	0.02	0.00025	124	1.55	7.02
HMJ02-07	1196	1787	1.49	0.134	0.02	0.02	0.00034	129	1.85	3.84
HMJ02-08	1130	513	0.45	0.166	0.02	0.02	0.00041	124	2.44	17.9
HMJ02-09	2467	1930	0.78	0.101	0.02	0.022	0.00034	142	2.02	7.97
HMJ02-10	830	910	1.1	0.25	0.02	0.022	0.00042	135	2.39	2.15
HMJ02-11	371	139	0.37	0.122	0.02	0.02	0.00044	126	2.81	4.24
HMJ02-12	1616	677	0.42	0.186	0.01	0.02	0.00042	124	2.54	5.77
HMJ02-13	872	236	0.27	0.209	0.01	0.023	0.00037	141	2.33	42
HMJ02-14	553	650	1.18	0.163	0.04	0.021	0.00072	134	4.15	7.28
HMJ02-15	692	373	0.54	0.217	0.04	0.022	0.00053	136	2.82	3.71
HMJ02-16	809	601	0.74	0.125	0.05	0.022	0.00062	142	3.22	9.43
HMJ02-17	2790	1987	0.71	0.125	0.01	0.02	0.00022	126	1.31	9.4
HMJ02-18	668	401	0.6	0.088	0.03	0.022	0.00056	144	3.43	24.3
HMJ02-19	1304	1450	1.11	0.189	0.03	0.02	0.00037	127	1.8	3.72
HMJ02-20	948	1096	1.16	0.143	0.02	0.022	0.00026	142	1.46	4.27
HMJ02-21	1315	620	0.47	0.163	0.02	0.02	0.00032	126	1.86	10.6
HMJ02-22	583	263	0.45	0.131	0.02	0.022	0.00036	141	2.28	20.1

with a large range of LREEs, especially La (Figure 9). The ratio of Ce(IV)/Ce(III) ranges from 2.30 to 42.0 (Table 3). The younger zircon group shows a small range of Ce(IV)/Ce(III) ratios (Figure 10), whereas the older zircon group shows a relatively larger range of Ce(IV)/Ce(III) ratios. The low Ce(IV)/Ce(III) ratio indicates that the Huangmeijian granite formed at low oxygen fugacity (Ballard *et al.* 2002; Liang *et al.* 2006). The large range of Ce(IV)/Ce(III) ratios of the older zircon group is likely due to capturing zircon grains of different origins, for example high oxygen fugacity adakitic intrusions (Xie *et al.* 2009) and other rocks of similar ages. Titanium concentration in the zircons ranges from 2.99 to 831 ppm, with younger zircons showing relatively low Ti concentrations. According to Ti concentrations and the formula of Watson *et al.* (2006), calculated temperatures of zircon formation range from 720°C to 1140°C. Zircons with younger ages have a smaller temperature range (720–820°C) as shown in Figure 11. By contrast, the older zircon group has a larger range of temperature, which again suggests its diverse origins, that is, inherited or captured.

Petrogenesis and tectonic implications

The Huangmeijian Pluton: an A-type affinity

The term 'A-type granite' was first proposed by Loiselle and Wones (1979) to distinguish a special group of granitic rocks that occurs in an extensional tectonic environment like rift zones or anorogenic settings. This group of granite shares common characteristics of high $FeO_T/(FeO_T + MgO)$ and K_2O/Na_2O ratios, high K_2O content, and enrichment of incompatible elements such as REEs (except Eu), Zr, Nb, and Ta. A-type granite also has high TiO_2/MgO ratios (Douce 1997). Concentrations of Ba, Sr, and Eu, as well as water fugacity, are low for A-type granite (Loiselle and Wones 1979).

The Huangmeijian granite has all the geochemical characteristics of A-type granite. It contains high total alkalis ($K_2O + Na_2O$ = 8.90–12.1 wt.%) and plots into the alkaline area of the SiO_2–AR diagram (Figure 12). ACNK ranges from 0.96 to 1.15, showing a metaluminous-peraluminous nature. The high Fe* [$FeO_T/(FeO_T + MgO)$ = 0.93–0.99] of the Huangmeijian granite is also a typical characteristic of A-type granite.

The trace element composition of the Huangmeijian granite also shows characteristics of A-type granites. The Huangmeijian granite is enriched in HFSE (Zr, Nb, Y) and REEs, whereas depleted in Ba, Sr, P, Ti, and Eu. The total concentrations of Nb, Zr, Ce, and Y (549–1489 ppm) > 350 ppm and the Nb/Ta (10.4–17.6) and Zr/Hf (25.1–71.5) ratios also show characteristics of A-type granites. The ratio of Y/Nb (0.49–0.81) indicates an intraplate formation environment and mainly mantle origin (Eby 1992).

Various discrimination diagrams are used to constrain their genetic environment and discriminate A-type granite from other kinds of granite. In the Pearce diagram, samples from the Huangmeijian granite are plotted in the within-plate area (Pearce *et al.* 1984) (Figure 13A), and they are mainly formed in the rift valley environment as shown in Figure 13. In FeO_T/MgO, Nb, Zr versus 10,000 Ga/Al diagrams, all Huangmeijian granite samples are plotted into the A-type granite area except for two samples (Figure 13B–D), and are characterized by high FeO_T/MgO ratio and high 10,000 Ga/Al ratio (2.95–3.91). These are typical characteristics of A-type granite.

Petrogenesis of the Huangmeijian granite

Although A-type granite is generally attributed to extensional environment, its petrogenesis is still controversial. One model proposed that A-type granite is the result of fractionation

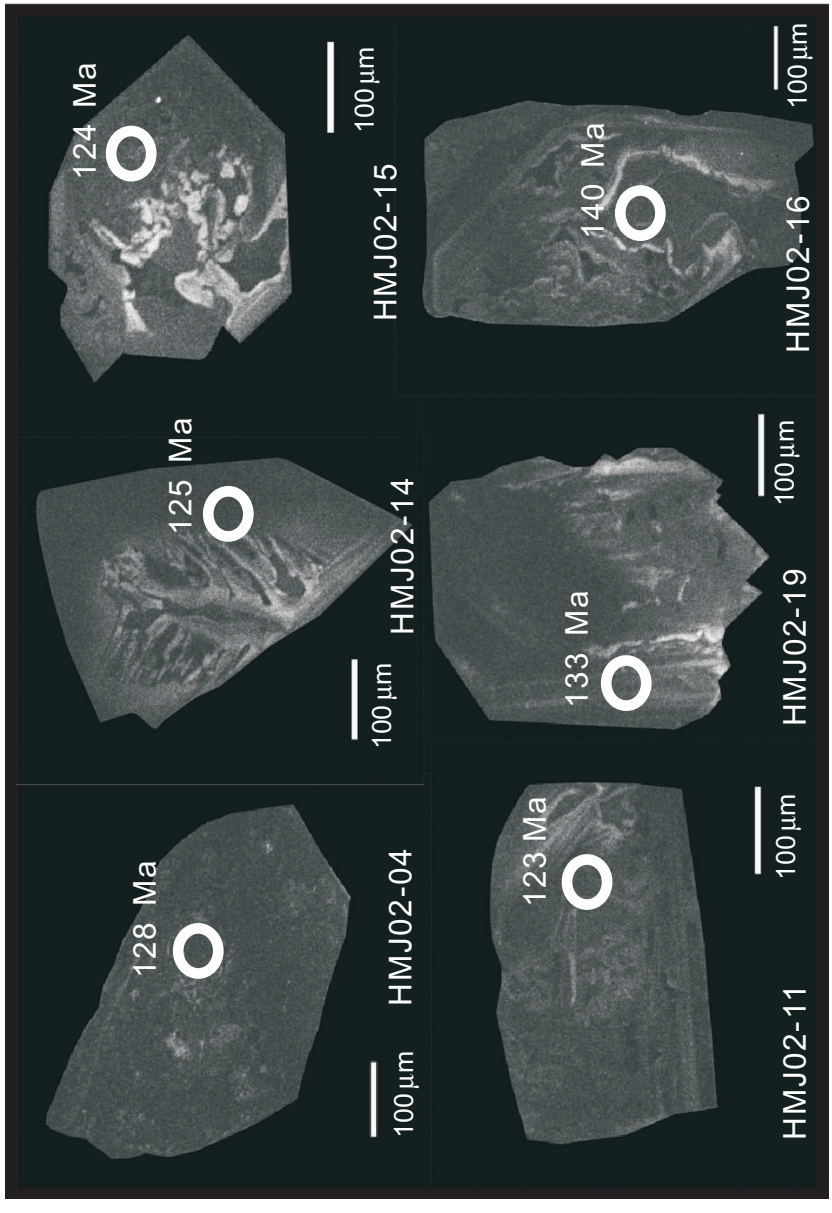

Figure 7. CL images of representative zircon grains for the Huangmeijian granite. The dark colour is likely due to high Th, U concentrations.

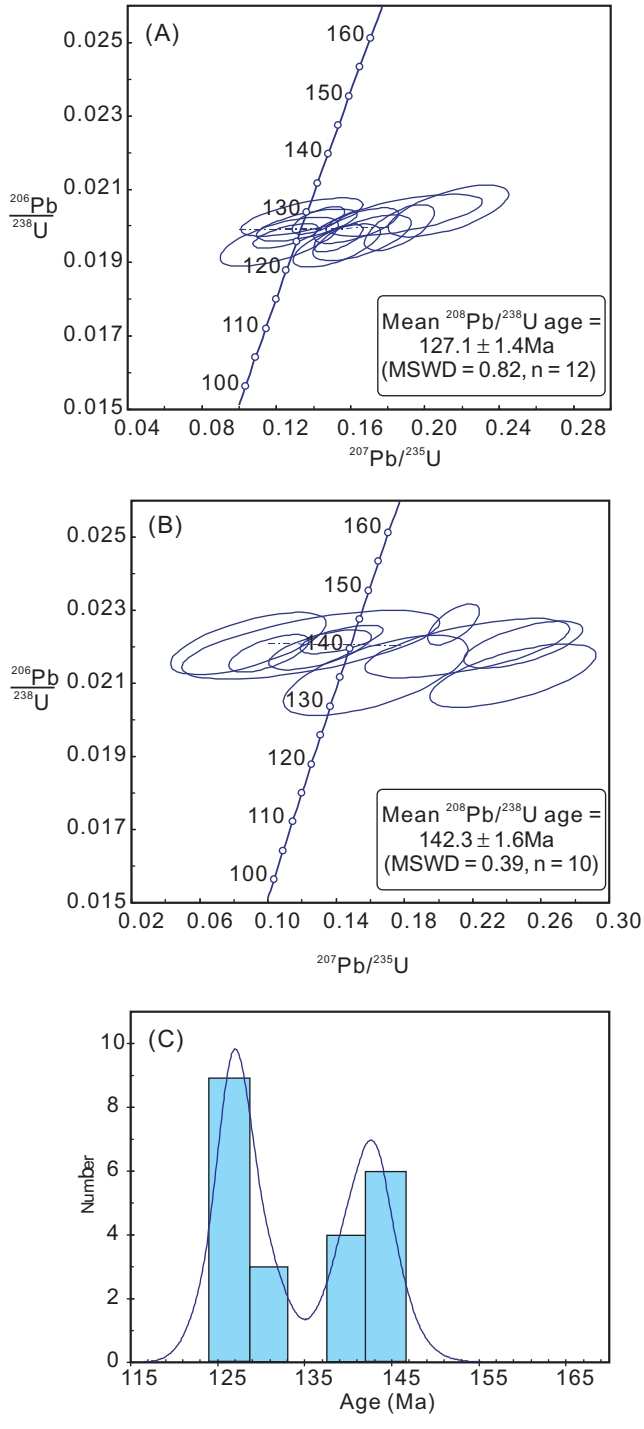

Figure 8. (A) Concordia diagram of the Huangmeijian granite (08HMJ02). The weighted mean $^{206}Pb/^{238}U$ age is 127.1 ± 1.4 Ma. (B) Concordia diagram of the Huangmeijian granite (08HMJ02). The weighted mean $^{206}Pb/^{238}U$ age is 142.3 ± 1.6 Ma. (C) Histograms of weighted mean $^{206}Pb/^{238}U$ age for zircons from the Huangmeijian granite. Given that all the zircons have high Th/U, such that they are magmatic, the younger group represents the crystallization of the Huangmeijian granite.

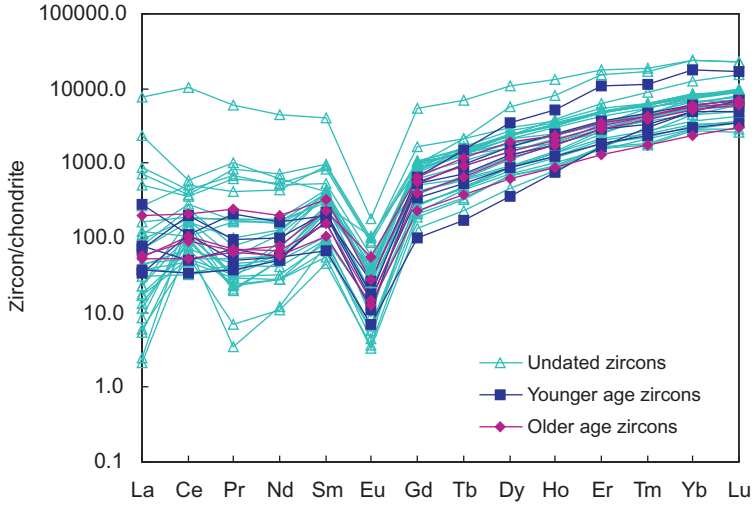

Figure 9. Zircon chondrite-normalized REE diagram for the Huangmeijian granite.

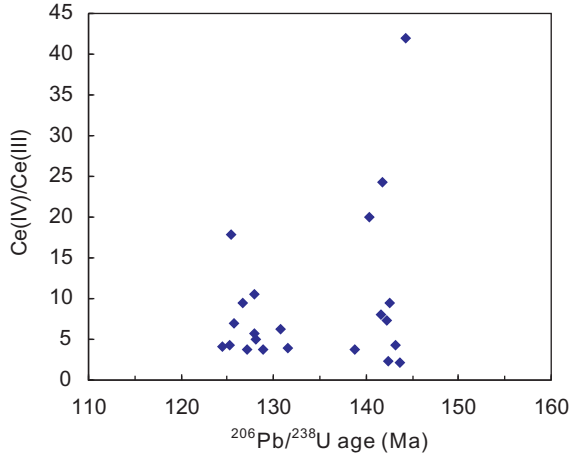

Figure 10. Zircon Ce(IV)/Ce(III) versus $^{206}Pb/^{238}U$ age diagram for the Huangmeijian granite.

of basaltic magmas, with or without crustal contamination (Loiselle and Wones 1979; Turner *et al.* 1992; Smith *et al.* 1999; Anderson *et al.* 2003). Another model attributed it to the melting of deep crust materials such as granulitic meta-igneous sources that were previously depleted by extraction of a hydrous felsic melt (Collins *et al.* 1982; Clemens *et al.* 1986; Whalen *et al.* 1987). The later model conflicts with the fact that A-type granite has high TiO_2/MgO and K_2O/Na_2O ratios (Creaser *et al.* 1991; Douce 1997). Experimental results suggest that the refractory granulitic residues from partial melting of a wide range of crustal rocks are characteristically depleted in alkalis relative to Al and depleted in TiO_2 relative to MgO (Creaser *et al.* 1991; Douce 1997). Re-melting of these residues cannot produce granitic liquids with the high $(Na_2O + K_2O)/Al_2O_3$ and TiO_2/MgO ratios that are characteristic of A-type granite. Moreover, to produce granites containing chemical and isotopic signatures of both mantle and crust, various models have been proposed, for example, fractionation of variously contaminated, mantle-derived alkali basalt (Bonin

Table 4. Zircon trace element data for Huangmeijian granite (ppm).

Sample	HMJ01	HMJ02	HMJ03	HMJ04	HMJ05	HMJ06	HMJ07	HMJ08	HMJ09	HMJ10	HMJ11	HMJ12	HMJ13	HMJ14	HMJ15
Y	16,249	2,541	2,066	2,015	5,433	3,947	7,154	4,458	1,835	7,922	7,596	20,483	2,676	2,297	6,118
Zr	481,778	482,421	481,306	484,425	482,657	481,195	481,195	481,195	481,195	481,232	482,180	482,135	482,462	483,125	483,142
Nb	80.1	45.6	40.2	45	43.2	269	48.6	29.8	69.9	18	82.5	231	62.1	25.6	96
Mo	0.68	0.47	0.29	1.73	0.55	5.43	1.88	0.55	1.67	0.43	4.18	3.65	0.4	0.14	3.34
Zr	81,894	81,150	84,238	75,607	78,781	79,800	78,922	71,896	80,656	69,554	75,210	72,447	75,624	76,776	74,409
La	7.08	10.3	4.14	9.47	10.9	563	64.2	25.7	8.7	4.08	2.01	1,785	5.47	3.2	38.1
Ce	20.1	44.1	40.3	20.6	32.9	358	317	177	29.6	31.8	92	6,454	68.3	54.4	118
Pr	3.72	4.39	2.22	4.12	4.91	96.52	39.78	16.08	2.82	3.1	1.82	563.77	2.88	2.16	16.6
Nd	27.3	22.9	12.6	19.6	27.6	293	203	84	12.7	26.4	23.4	2,072	15	13.2	72.3
Sm	37.7	16	10.4	14.5	34.6	65	144	65.9	8.39	40.5	34	617	12.9	14.3	50.8
Eu	2.27	0.72	0.33	0.75	2.25	1.47	5.17	2.19	0.19	5.98	0.53	10.52	0.39	0.33	2.49
Gd	196	57.4	44.2	46	153	85.8	349	184	27.3	175	162	1,113	55.4	59.3	160
Tb	81.1	17.5	12.6	16.4	49.6	23.5	79.9	46.2	8.5	63.8	50	261.9	18.5	17.7	56.9
Dy	1,422	228	178	186	535	285	775	455	119	700	583	2,728	225	206	629
Ho	457	68.8	51.1	58.2	143	105	208	135	45.2	199	214	762	76.5	65.4	181
Er	2,535	330	275	253	587	553	916	558	271	799	1,063	2,890	346	298	758
Tm	423	61.8	47.3	54.8	109	138	158	109	66.6	146	222	486	70	58.3	150
Yb	4,096	565	480	491	923	1,309	1,476	934	755	1,123	2,165	3,990	611	525	1,306
Lu	578	90.4	71.4	88.3	149	239	231	168	154	179	398	576	106	93.4	225
Hf	11,385	14,106	14,046	15,288	14,107	15,160	8,202	8,250	10,314	9,758	9,605	9,098	11,563	10,694	11,250
Ta	15	17.6	12.3	29.4	24.3	92.7	9.4	7.2	22	6.6	11.9	72.3	13.7	8.3	33.2
Pb	390	175	157	152	170	464	242	164	277	51	414	533	139	128	195
Th	664	1,286	1,116	533	1,163	12,897	7,474	4,408	1,911	447	2,534	12,845	974	983	2,272
U	5,133	2,310	2,155	1,852	2,263	6,325	3,487	2,353	3,461	551	4,951	7,965	1,696	1,617	2,443
Ti	19.09	8.11	4.61	128.15	5.02	94.39	41.14	24.2	30.49	10.94	2.99	13.29	94.85	8.21	66.08
T (°C)	801	723	677	1,029	684	986	883	825	849	749	645	767	987	724	939

Sample	HMJ16	HMJ17	HMJ18	HMJ19	HMJ20	HMJ21	HMJ22	HMJ23	HMJ24	HMJ25	HMJ26	HMJ27	HMJ28	HMJ29	HMJ30
Y	6,223	3,790	2,820	3,055	3,649	4,401	6,120	6,724	3,930	6,248	4,497	5,476	11,751	1,598	2,423
Zr	481,195	481,195	481,195	481,195	481,195	481,195	482,730	480,820	483,358	483,760	479,290	483,233	482,139	481,195	481,786
Nb	22.6	113	147	193	35.3	8.1	18.4	18	11.8	13.2	106	19.3	83.8	96.3	46.4
Mo	0.3	5.3	5.4	8.31	bdl	0.26	0.3	1.74	0.18	0.2	2.99	0.48	1.41	0.7	0.84
Zr	74,016	79,080	68,653	74,751	76,480	73,711	80,889	71,679	76,919	76,211	71,416	72,942	81,178	71,091	74,201
La	18.6	173	22.6	212	0.51	2.67	5.38	28.8	1.28	0.59	124	16.4	8.83	18.1	67.3
Ce	147	227	109	274	48.1	64.7	104	64.8	61.5	99.3	222	98.1	20.6	30.6	66.4
Pr	7.52	80.3	17.3	63.8	0.33	3.28	5.23	15.2	1.97	2.79	59.5	9.7	3.48	6.72	20.4
Nd	57	344	80.3	234	5.6	34.5	50.3	75.2	23.8	43.1	247	60.3	23.4	25.4	76.4
Sm	60.7	149	44.8	81.7	12.3	40.2	56.3	61.3	33.6	58.4	125	59.9	29.7	10.2	30.7
Eu	1.76	5.75	1.96	3.38	0.26	1.07	1.48	2.73	1	1.84	4.97	1.78	1.5	0.41	0.89
Gd	224	216	87.4	107	76.9	150	201	189	127	222	208	204	237	20.8	69.6
Tb	57.7	47.8	21.8	23.6	26	40.3	53.2	54.9	34.1	57.9	50.3	51.7	57.3	6.4	20
Dy	597	404	222	236	317	419	587	612	369	603	470	549	903	94	218
Ho	184	104	76.4	82.1	109	134	178	189	118	190	131	169	294	41.9	69
Er	777	440	401	456	477	573	809	832	511	812	568	720	1,825	270	300
Tm	150	95.9	104	115	92.5	112	151	164	102	159	122	142	290	75.7	60.7
Yb	1,293	925	1,057	1,216	763	982	1,379	1,423	885	1,366	1,115	1,216	3,044	831	521
Lu	236	167	208	252	128	185	233	229	163	254	198	225	423	174	88.9
Hf	7,912	13,091	12,381	8,786	12,835	8,341	8,180	7,300	8,594	8,116	9,666	8,162	11,240	10,100	10,130
Ta	5.2	58.8	59	42.7	9.2	2.3	6.3	7.6	3.6	3.1	25.4	4.1	17.9	33.6	12.6
Pb	155	314	371	403	155	77	129	89	91	105	219	125	373	250	128
Th	2,960	12,780	15,622	4,684	787	799	1,438	764	802	1,400	3,697	2,148	406	1,421	770
U	1,996	4,195	5,872	5,108	1,842	838	1,449	895	923	1,157	3,603	1,207	4,852	3,450	1,440
Ti	21.57	78.42	32.09	831.45	5.84	13.34	12.51	361.75	13.19	16.44	82.58	17.25	24.14	7.98	12.88
T (°C)	813	961	855	1,371	696	767	761	1,199	766	787	968	791	825	722	764

(*Continued*)

Table 4. (*Continued*)

Sample	HMJ31	HMJ32	HMJ33	HMJ34	HMJ35	HMJ36	HMJ28	HMJ29	HMJ30	HMJ31	HMJ32	HMJ33	HMJ34	HMJ35	HMJ36
Y	3,793	4,877	1,854	4,081	3,595	5,077	11,751	1,598	2,423	3,793	4,877	1,854	4,081	3,595	5,077
Zr	481,985	482,462	481,195	481,195	481,195	481,971	482,139	481,195	481,786	481,985	482,462	481,195	481,195	481,195	481,971
Nb	83.4	54.4	32.1	133	83.9	72.8	83.8	96.3	46.4	83.4	54.4	32.1	133	83.9	72.8
Mo	0.5	0.3	0.41	1.11	0.97	1.66	1.41	0.7	0.84	0.5	0.3	0.41	1.11	0.97	1.66
Zr	86,153	75,574	80,052	71,230	77,442	81,235	81,178	71,091	74,201	86,153	75,574	80,052	71,230	77,442	81,235
La	16.7	7.91	12.5	47.8	13.4	13.7	8.83	18.1	67.3	16.7	7.91	12.5	47.8	13.4	13.7
Ce	121	67.6	32.4	129	65.6	56.5	20.6	30.6	66.4	121	67.6	32.4	129	65.6	56.5
Pr	8.85	4.81	6.15	23.1	6.7	6.48	3.48	6.72	20.4	8.85	4.81	6.15	23.1	6.7	6.48
Nd	46.6	26.3	27	92.7	32.1	37.3	23.4	25.4	76.4	46.6	26.3	27	92.7	32.1	37.3
Sm	33.8	24.7	16.3	50.5	24.4	35.8	29.7	10.2	30.7	33.8	24.7	16.3	50.5	24.4	35.8
Eu	1.03	0.64	0.73	1.6	0.85	3.23	1.5	0.41	0.89	1.03	0.64	0.73	1.6	0.85	3.23
Gd	108	109	47.4	117	80.6	137	237	20.8	69.6	108	109	47.4	117	80.6	137
Tb	27.6	36.3	14.2	34.3	24.4	43.3	57.3	6.4	20	27.6	36.3	14.2	34.3	24.4	43.3
Dy	336	422	162	362	295	491	903	94	218	336	422	162	362	295	491
Ho	97.9	139.7	50.1	114	97.4	134	294	41.9	69	97.9	139.7	50.1	114	97.4	134
Er	467	616	221	521	467	586	1,825	270	300	467	616	221	521	467	586
Tm	83.1	122	45.7	111	97.7	111	290	75.7	60.7	83.1	122	45.7	111	97.7	111
Yb	821	1,028	409	1,014	886	986	3,044	831	521	821	1,028	409	1,014	886	986
Lu	126	175	75	178	152	163	423	174	88.9	126	175	75	178	152	163
Hf	11,218	11,263	13,918	14,311	12,052	11,080	11,240	10,100	10,130	11,218	11,263	13,918	14,311	12,052	11,080
Ta	20	12.3	16.1	52	25.3	28.6	17.9	33.6	12.6	20	12.3	16.1	52	25.3	28.6
Pb	260	181	140	271	293	175	373	250	128	260	181	140	271	293	175
Th	3,241	1,237	797	4,376	3,487	1,027	406	1,421	770	3,241	1,237	797	4,376	3,487	1,027
U	3,715	2,331	1,865	3,971	4,047	2,206	4,852	3,450	1,440	3,715	2,331	1,865	3,971	4,047	2,206
Ti	7.92	8.8	39.1	42.9	8.21	265	24.14	7.98	12.88	7.92	8.8	39.1	42.9	8.21	265
T (°C)	721	730	877	887	724	1,143	825	722	764	721	730	877	887	724	1,143

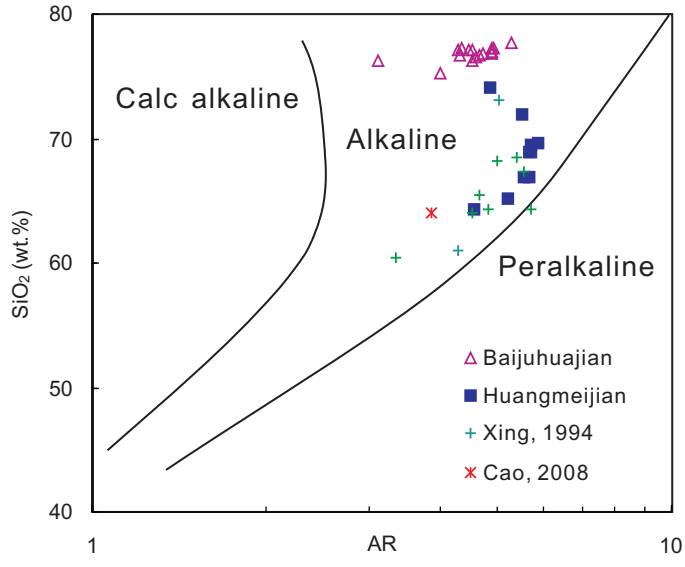

Figure 11. SiO_2–AR diagram for the Huangmeijian granite.

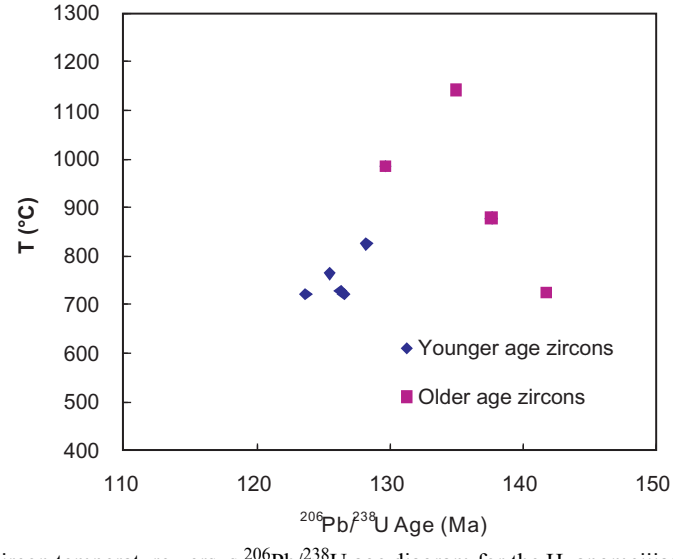

Figure 12. Zircon temperature versus $^{206}Pb/^{238}U$ age diagram for the Huangmeijian granite.

2007), mixing of crustal melts with OIB magma (Eby 1990, 1992), and evolution of mantle-derived mafic and intermediate magmas (Turner *et al.* 1992).

Major and trace element compositions of the Huangmeijian A-type granite give constraints on its origin. The overall high and large ranges of Nb (71.8–118 ppm), Ta (4.32–8.05 ppm) concentrations, as well as low Y/Nb (0.49–0.81) ratios and Zr concentration, indicate an origin of mantle source with a little crustal contamination. Given that the crust has a higher ratio of Y/Nb (>2), crustal contamination increases the value of Y/Nb (Eby 1992). The incompatible element ratio diagrams show that the Huangmeijian A-type

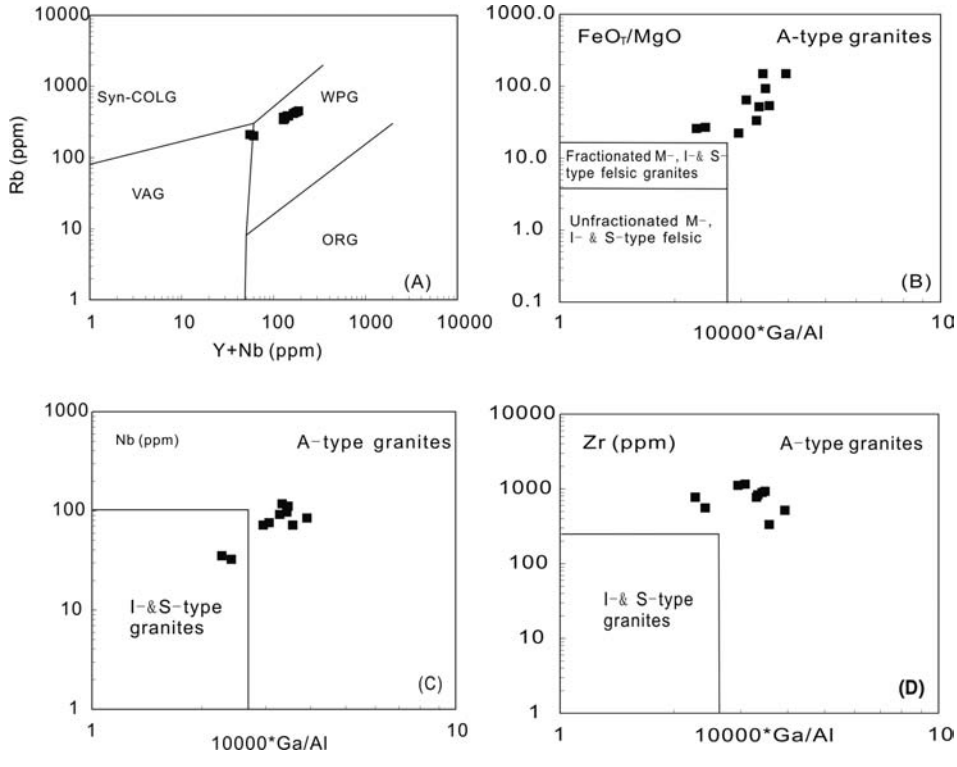

Figure 13. (A) Discrimination diagrams for granites (Pearce *et al.* 1984). The Huangmeijian granites are plotted in the field of WPG (= within-plate granite). (B) FeO_T/MgO versus 10,000 Ga/Al diagram (Whalen *et al.* 1987). The Huangmeijian granitic samples are plotted in the field of A-type granite. (C and d) Discrimination diagrams for granites (Whalen *et al.* 1987). Samples of the Huangmeijian granite are plotted into the area of A-type granites.

granite has chemical characteristics similar to OIB (Figure 14). This also indicates magma origin from the enriched mantle with little crustal contamination during mantle upwelling. The Nd isotope characteristics of the Huangmeijian A-type granite also support the enriched mantle source origin, with ε_{Nd} of –2.50 (Xing and Xu 1994).

Regional extension and tectonic evolution of the LYRB

The geodynamic mechanism for the formation of A-type granite in the LYRB is controversial. One proposed model is that A-type granite in the LYRB formed in back-arc and post-collision extension settings related to the Triassic collision between the North and South China blocks (Du *et al.* 2007; Cao *et al.* 2008). The Triassic collision, however, occurred in the Qinling-Dabie orogenic belt (Meng and Zhang 1999; Li *et al*. 2000; Sun *et al*. 2002; Zheng *et al*. 2003; Zhou *et al*. 2008c), whereas A-type granites distribute mainly in the LYRB (Xing and Xu 1994; Fan *et al.* 2008; Ling *et al.* 2009; Wong *et al*. 2009). It is difficult to form A-type granite up to several hundred kilometres away from the orogenic belt after about 100 Ma through post-collisional extension. Alternatively, the extension environment has been attributed to an intracontinental shearing associated with mantle upwelling (Fan *et al.* 2008; Zhou *et al.* 2008a, 2008b). This model, however, does not explain why mantle upwelling occurred within a short period of time (only 2–3 Ma). Some

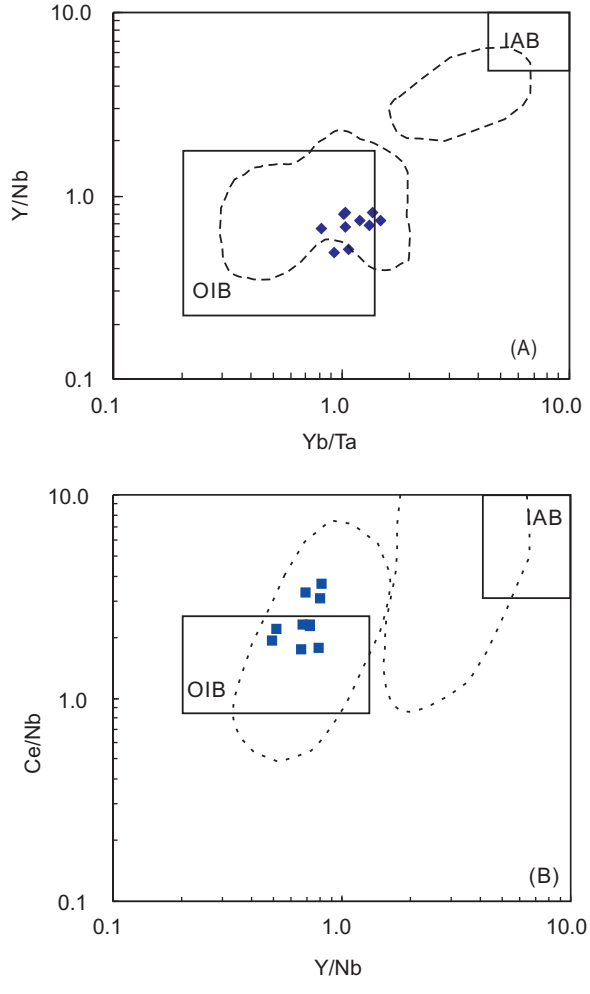

Figure 14. (A) Yb/Ta versus Y/Nb and (B) Y/Nb versus Ce/Nb diagrams for the Huangmeijian granite (Eby 1992). OIB = oceanic island basalt; IAB = island arc basalt. Fields with dashed lines represent A1- and A2-type granites of Eby (1990).

A-type granite rocks in the eastern part of the region were assumed to be the result of slab rollback (Wong *et al.* 2009) based on the drifting history of the Pacific plate (Koppers *et al*. 2001; Sun *et al*. 2007). The Pacific plate may have started to subduct underneath eastern China during the Late Jurassic (Zhou and Li 2000; Li and Li 2007; Wang *et al*. 2011), but a simple slab rollback model cannot plausibly explain why A-type granites in the LYRB formed within a short period of time in the Early Cretaceous and distributed linearly from west to east. Moreover, none of these models paid any detailed attention to adakites and other rocks of the Early Cretaceous in the region, which are spatially closely associated with but slightly predate A-type granites. Based on the distribution of adakite, A-type granite, and Nb-enriched volcanic rocks, a ridge subduction model has also been proposed (Ling *et al.* 2009). According to this model, A-type granites formed when a slab window opened during the late stage of the ridge subduction (Ling *et al.* 2009).

From the Late Jurassic to the Early Cretaceous, there were two plates subducting under eastern China. They were the Pacific plate, subducting towards the southwest, and the Izanagi plate subducting towards the northwest (Maruyama *et al.* 1997, Sun *et al.* 2007). Because of the different directions and different velocities between the Pacific and the Izanagi plates, the ridge between these two plates moved westward during the subduction and subducted under the Lower Yangtze River region at about 140 Ma. The ridge gradually opened as the subduction continued, forming a slab window and consequently, A-type granites (Ling *et al.* 2009). The asthenospheric mantle is characterized by dry and high temperatures. Previous studies on ridge subduction have already suggested that A-type granite associated with ridge subduction probably resulted from asthenospheric mantle material upwelling through the slab window and evolved at shallow crust in low pressure condition (Thorkelson and Breitsprecher 2005).

The Huangmeijian A-type granite has the characteristics of high genesis temperature, with oxygen fugacity lower than that of adakites in the region. We suggest that the Huangmeijian A-type granite resulted from the ridge subduction. During the ridge subduction, the ridge between the Pacific and the Izanagi plates opened; consequently, enriched mantle materials melted due to hot mantle materials upwelling through the slab window.

Previous dating results showed that Huangmeijian A-type granite (125.4 ± 1.7 Ma; Fan *et al.* 2008) formed at exactly the same time as the Baijuhuajian A-type granite (125.6 ± 3.2 Ma; Wong *et al*. 2009), several hundred kilometres to the east. Interestingly, the K–Ar age of the Huangmeijian granite is identical to its zircon U–Th age (Zheng 1995). Considering the high temperature of the Huangmeijian granite, this is unusual. Our new result (127.1 ± 1.4 Ma) is marginally older than previous results. The age difference between our result and that of Baijuhuajian A-type granite is 1.5 Ma, which is about the same as the 2σ error of our result and the 1σ error of the Baijuhuajian age. This suggests that the age difference is real at a confidence level of approximately 60%. This is consistent with the ridge subduction model as the slab window opened from the west and migrated eastward.

As mentioned above, compared to the geochemical characteristics of the Baijuhuajian A-type granite, the Huangmeijian granite is enriched in LREEs and depleted in HREEs with lower SiO_2, indicating a more enriched mantle source for the Huangmeijian granite. Enriched mantle source was common in eastern China before 110 Ma (Xu 2001, 2006). Given that the Baijuhuajian granite is located in the east, closer to the subduction zone, it is likely that more enriched mantle materials there were removed by early subduction, such that the granite itself is less enriched compared to Huangmeijian.

Conclusions

Geochemical data indicate that the Huangmeijian granite, exposed along the northern bank of the LYRB, is a typical A-type granite characterized by high Fe* (FeO_T/(FeO_T + MgO)), enrichments of incompatible elements [REEs (except Eu), Zr, Nb, and Ta], and depletion in Ba, Sr, and Eu. High genesis temperature and low oxygen fugacity are consistent with its mantle origin. Negative ε_{Nd} values indicate the evolvement of enriched mantle ± crustal materials. Zircon U–Pb ages of the Huangmeijian A-type granite range from 127 to 142 Ma, which can be classified into two groups with the younger representing its crystallization age (127 Ma). Together with previous studies, we suggest that the genesis of Huangmeijian A-type granite was due to the slab window related to a Cretaceous ridge subduction in the LYRB, which opened at ≥127 Ma.

Acknowledgements

The contribution is supported by the Key Research project of the Chinese Academy of Sciences (KZCX1-YW-15), Ministry of Science and Technology of China (2006CB403505), and the Natural Science Foundation of China (No. 40525010). We thank Ying Liu (Guangzhou Institute of Geochemistry, Chinese Academy of Sciences) for assistance in fieldwork and analysis of XRF and ICP-MS. Constructive review comments from Zhaochong Zhang and Taofa Zhou are sincerely thanked. Contribution No. IS-1203 from GIGCAS.

References

Anderson, I.C., Frost, C.D., and Frost, B.R., 2003, Petrogenesis of the Red Mountain pluton, Laramie anorthosite complex, Wyoming: implications for the origin of A-type granite: Precambrian Research, v. 124, p. 243–267.

Ballard, J.R., Palin, J.M., and Campbell, I.H., 2002, Relative oxidation states of magmas inferred from Ce(IV)/Ce(III) in zircon: Application to porphyry copper deposits of northern Chile: Contributions to Mineralogy and Petrology, v. 144, p. 347–364.

Belousova, E.A., Griffin, W.L., Suzanne, Y.O.R., and Fisher, N.I., 2002, Igneous zircon: Trace element composition as an indicator of source rock type: Contributions to Mineralogy and Petrology, v. 143, p. 602–622.

Bonin, B., 2007, A-type granites and related rocks: Evolution of a concept, problems and prospects: Lithos, v. 97, p. 1–29.

Cao, Y., Du, Y.S., Cai, C.L., Qin, X.L., Li, S.T., and Xiang, W.S., 2008, Mesozoic A-type granitoids and xenoliths in the Lujiang-Zongyang area, Anhui Province: Significance in post-collisional magmatic evolution: Geological Journal of China Universities, v. 4, p. 565–576 (in Chinese with English abstract).

Chang, Y.F., Liu, X.P., and Wu, Y.C., 1991, The copper-iron belt of the lower and middle reaches of the Changjiang River: Beijing, Geological Publishing House, 379 p (in Chinese).

Chen, J.F., and Jahn, B.M., 1998, Crustal evolution of southeastern China: Nd and Sr isotopic evidence: Tectonophysics, v. 284, p. 101–133.

Chen, J.F., Yan, J., Xie, Z., Xu, X., and Xing, F., 2001, Nd and Sr isotopic compositions of igneous rocks from the lower Yangtze region in eastern China: Constraints on sources: Physics and Chemistry of the Earth Part a-Solid Earth and Geodesy, v. 26, p. 719–731.

Clemens, J.D., Holloway, J.R., and White, A.J.R., 1986, Origin of an A-type granite experimental constraints: American Mineralogist, v. 71, p. 317–324.

Collins, W.J., Beams, S.D., White, A.J.R., and Chappell, B.W., 1982, Nature and origin of A-type granites with particular reference to southeastern Australia: Contributions to Mineralogy and Petrology, v. 80, p. 189–200.

Creaser, R.A., Price, R.C., and Wormald, R.J., 1991, A-type granites revisited assessment of a residual source model: Geology, v. 19, p. 163–166.

Deng, J.F., Dai, S.Q., Zhao, H.L., and Du, J.G., 2002, Recognition of magma-fluid-metallogenic system and subsystem in the Tongling Cu–Au (Ag) metallogenic area: Mineralium Deposita, v. 21, p. 317–322.

Ding, X., Lundstrom, C., Huang, F., Li, J., Zhang, Z.M., Sun, X.M., Liang, J.L., and Sun, W.D., 2009, Natural and experimental constraints on formation of the continental crust based on niobium-tantalum fractionation: International Geology Review, v. 51, p. 473–501.

Douce, A.E.P., 1997, Generation of metaluminous A-type granites by low-pressure melting of calc-alkaline granitoids: Geology, v. 25, p. 743–746.

Du, Y.S., Cao, Y., Yuan, W.M., Lou, Y.E., Li, S.T., and Lu, X., 2007, Mesozoic post-collisional to postorogenic magmatic activities and crustal interaction with mantle along the Yangtze River, Anhui province: evidence from volcanic-intrusive complexes and xenoliths: Acta Petrologica Sinica, v. 23, p. 1294–1301 (in Chinese with English abstract).

Eby, G.N., 1990, The A-type granitoids a review of their occurrence and chemical characteristics and speculations their petrogenesis: Lithos, v. 26, p. 115–134.

Eby, G.N., 1992, Chemical subdivision of the A-type granitoids petrogenetic and tectonic implications: Geology, v. 20, p. 641–644.

Fan, Y., Zhou, T.F., Yuan, F., Qian, C.C., Lu, S.M., and Cooke, D.R., 2008, LA-ICP MS Zircon U–Pb Ages of the A-type granites in the Lu-Zong (Lujiang-Zongyang) area and their geological significances: Acta Petrologica Sinica, v. 24, p. 1715–1724 (in Chinese with English abstract).

Foley, S., Tiepolo, M., and Vannucci, R., 2002, Growth of early continental crust controlled by melting of amphibolite in subduction zones: Nature, v. 417, p. 837–840.

Green, T.H., 1995, Significance of Nb/Ta as an indicator of geochemical processes in the crust-mantle system: Chemical Geology, v. 120, p. 347–359.

Huang, D.Z., Wang, X.Y., Yang, X.Y., Li, G.M., Huang, S.Q., Liu, Z., Peng, Z.H., and Qiu, R.L., 2011, Geochemistry of gold deposits in the Zhangbaling Tectonic Belt, Anhui Province, China: International Geology Review, v. 53, p. 612–634.

Hoskin, P.W.O., and Black, L.P., 2000, Metamorphic zircon formation by solid-state recrystallization of protolith igneous zircon: Journal of Metamorphic Geology, v. 18, p. 423–439.

Koppers, A.A.P., Morgan, J.P., Morgan, J.W., and Staudigel, H., 2001, Testing the fixed hotspot hypothesis using Ar-40/Ar-39 age progressions along seamount trails: Earth and Planetary Science Letters, v. 185, p. 237–252.

Li, S.G., Jagoutz, E., Chen, Y.Z., and Li, Q.L., 2000, Sm–Nd and Rb-Sr isotopic chronology and cooling history of ultrahigh pressure metamorphic rocks and their country rocks at Shuanghe in the Dabie Mountains, Central China: Geochimica et Cosmochimica Acta, v. 64, p. 1077–1093.

Li, Z.X., and Li, X.H., 2007, Formation of the 1300-km-wide intracontinental orogen and postorogenic magmatic province in Mesozoic South China: A flat-slab subduction model: Geology, v. 35, p. 179–182.

Liang, H.Y., Campbell, I.H., Allen, C., Sun, W.D., Liu, C.Q., Yu, H.X., Xie, Y.W., and Zhang, Y.Q., 2006, Zircon Ce4+/Ce3+ ratios and ages for Yulong ore-bearing porphyries in eastern Tibet: Mineralium Deposita, v. 41, p. 152–159.

Liang, J.L., Ding, X., Sun, X.M., Zhang, Z.M., Zhang, H., and Sun, W.D., 2009, Nb/Ta fractionation observed in eclogites from the Chinese Continental Scientific Drilling Project: Chemical Geology, v. 268, p. 27–40.

Ling, M.X., Wang, F.Y., Ding, X., Hu, Y.H., Zhou, J.B., Zartman, R.E., Yang, X.Y., and Sun, W.D., 2009, Cretaceous ridge subduction along the lower Yangtze River Belt, eastern China: Economic Geology, v. 104, p. 303–321.

Liou, J.G., Zhang, R.Y., Ernst, W.G., Liu, J., and McLimans, R., 1998, Mineral parageneses in the Piampaludo eclogitic body, Gruppo di Voltri, Western Ligurian Alps: Schweizerische Mineralogische Und Petrographische Mitteilungen, v. 78, p. 317–335.

Liu, Y., Liu, H.C., and Li, X.H., 1996, Simultaneous and precise determination of 40 trace elements in rock samples using ICP-MS: Geochimica, v. 25, p. 552–558 (in Chinese with English abstract).

Loiselle, M.C., and Wones, D.R., 1979, Characteristics of anorogenic granites: Geological Society of America Abstracts with Programs, v. 11, p. 468.

Ma, J.-L., Wei, G.-J., Xu, Y.-G., Long, W.-G., and Sun, W.-D., 2007, Mobilization and re-distribution of major and trace elements during extreme weathering of basalt in Hainan Island, South China: Geochimica et Cosmochimica Acta, v. 71, p. 3223–3237.

Manning, C.E., and Bohlen, S.R., 1991, The reaction titanite + kyanite = anorthite + rutile and titanite-rutile barometry in eclogites: Contributions to Mineralogy and Petrology, v. 109, p. 1–9.

Mao, J.W., Wang, Y.T., Lehmann, B., Yu, J.J., Du, A.D., Mei, Y.X., Li, Y.F., Zang, W.S., Stein, H.J., and Zhou, T.F., 2006, Molybdenite Re–Os and albite Ar-40/Ar-39 dating of Cu–Au–Mo and magnetite porphyry systems in the Yangtze River valley and metallogenic implications: Ore Geology Reviews, v. 29, p. 307–324.

Maruyama, S., Isozaki, Y., Kimura, G., and Terabayashi, M., 1997, Paleogeographic maps of the Japanese Islands: Plate tectonic synthesis from 750 Ma to the present: Island Arc, v. 6, p. 121–142.

Mcdonough, W.F., 1991, Partial melting of subducted oceanic-crust and isolation of its residual eclogitic lithology: Philosophical Transactions of the Royal Society of London Series a-Mathematical Physical and Engineering Sciences, v. 335, p. 407–418.

Meng, Q.R., and Zhang, G.W., 1999, Timing of collision of the North and South China blocks: Controversy and reconciliation: Geology, v. 27, p. 123–126.

Pan, Y.M., and Dong, P., 1999, The Lower Changjiang (Yangzi/Yangtze River) metallogenic belt, east central China: intrusion- and wall rock-hosted Cu–Fe–Au, Mo, Zn, Pb, Ag deposits: Ore Geology Reviews, v. 15, p. 177–242.

Pearce, J.A., Harris, N.B.W., and Tindle, A.G., 1984, Trace element discrimination diagrams for the tectonic interpretation of granitic rocks: Journal of Petrology, v. 25, p. 956–983.

Rudnick, R.L., Barth, M., Horn, I., and McDonough, W.F., 2000, Rutile-bearing refractory eclogites: Missing link between continents and depleted mantle: Science, v. 287, p. 278–281.
Smith, D.R., Noblett, J., Wobus, R.A., Unruh, D., Douglass, J., Beane, R., Davis, C., Goldman, S., Kay, G., Gustavson, B., Saltoun, B., and Stewart, J., 1999, Petrology and geochemistry of late-stage intrusions of the A-type, mid-Proterozoic Pikes Peak batholith (Central Colorado, USA): implications for petrogenetic models: Precambrian Research, v. 98, p. 271–305.
Streckeisen, A., and Le Maitre, R.W., 1979, A chemical approximation to the modal QAPF classification of igneous rocks: Neues Jahrbuch für Mineralogie, Abhandlungen, v. 136, p. 169–206.
Sun, W.D., Ding, X., Hu, Y.H., and Li, X.H., 2007, The golden transformation of the Cretaceous plate subduction in the west Pacific: Earth and Planetary Science Letters, v. 262, p. 533–542.
Sun, W.D., Zhang, H., Ling, M.X., Ding, X., Chung, S.L., Zhou, J.B., Yang, X.Y., and Fan, W.M., 2011, The genetic association of adakites and Cu–Au ore deposits: International Geology Review, v. 53, p. 691–703.
Sun, W.D., Ling, M.X., Yang, X.Y., Fan, W.M., Ding, X., and Liang, H.Y., 2010, Ridge subduction and porphyry copper gold mineralization: An overview: Science China: Earth Sciences, v. 53, p. 475–484.
Sun, W.D., Williams, I.S., and Li, S.G., 2002, Carboniferous and Triassic eclogites in the western Dabie Mountains, east-central China: Evidence for protracted convergence of the North and South China Blocks: Journal of Metamorphic Geology, v. 20, p. 873–886.
Sun, W.D., Xie, Z., Chen, J.F., Zhang, X., Chai, Z.F., Du, A.D., Zhao, J.S., Zhang, C.H., and Zhou, T.F., 2003, Os–Os dating of copper and molybdenum deposits along the middle and lower reaches of the Yangtze River, China: Economic Geology and the Bulletin of the Society of Economic Geologists, v. 98, p. 175–180.
Thorkelson, D.J., and Breitsprecher, K., 2005, Partial melting of slab window margins: Genesis of adakitic and non-adakitic magmas: Lithos, v. 79, p. 25–41.
Tu, X.L., Zhang, H.F., Deng, W.F., Liang, H.Y., and Sun, W.D., 2009, Application of RESOlution laser ablation ICPMS in trace element analyses: Geochimica (in press).
Turner, S.P., Foden, J.D., and Morrison, R.S., 1992, Derivation of some A-type magmas by fractionation of basaltic magma an example from the padthaway ridge, south Australia: Lithos, v. 28, p. 151–179.
Wang, F.Y., Ling, M.X., Ding, X., Hu, Y.H., Zhou, J.B., Yang, X.Y., Liang, H.Y., Fan, W.M., and Sun, W.D., 2011, Mesozoic large magmatic events and mineralization in SE China : oblique subduction of the Pacific plate: International Geology Review, v. 53, p. 704–726.
Wang, Q., Wyman, D.A., Xu, J., Jian, P., Zhao, Z., Li, C., Xu, W., Ma, J., and He, B., 2007, Early Cretaceous adakitic granites in the Northern Dabie Complex, central China: Implications for partial melting and delamination of thickened lower crust: Geochimica et Cosmochimica Acta, v. 71, p. 2609–2636.
Wang, Q., Wyman, D.A., Xu, J.F., Zhao, Z.H., Jian, P., Xiong, X.L., Bao, Z.W., Li, C.F., and Bai, Z.H., 2006, Petrogenesis of Cretaceous adakitic and shoshonitic igneous rocks in the Luzong area, Anhui Province (eastern China): Implications for geodynamics and Cu–Au mineralization: Lithos, v. 89, p. 424–446.
Wang, Q., Xu, J.F., Zhao, Z.H., Bao, Z.W., Xu, W., and Xiong, X.L., 2004a, Cretaceous high-potassium intrusive rocks in the Yueshan-Hongzhen area of east China: Adakites in an extensional tectonic regime within a continent: Geochemical Journal, v. 38, p. 417–434.
Wang, Y., Deng, J.F., and Ji, G.Y., 2004b, A perspective on the geotectonic setting of early Cretaceous adakite-like rocks in the lower reaches of Yangtze River and its significance for copper–gold mineralization: Acta Petrologica Sinica, v. 20, p. 297–314.
Watson, E.B., Wark, D.A., and Thomas, J.B., 2006, Crystallization thermometers for zircon and rutile: Contributions to Mineralogy and Petrology, v. 151, p. 413–433.
Whalen, J.B., Currie, K.L., and Chappell, B.W., 1987, A-type granites geochemical characteristics, discrimination and petrogenesis: Contributions to Mineralogy and Petrology, v. 95, p. 407–419.
Wong, J., Sun, M., Xing, G., Li, X.H., Zhao, G., Wong, K., Yuan, C., Xia, X., Li, L., and Wu, F., 2009, Geochemical and zircon U–Pb and Hf isotopic study of the Baijuhuajian metaluminous A-type granite: Extension at 125–100 Ma and its tectonic significance for South China: Lithos, v. 112, p. 289–305.
Xiao, Y.L., Sun, W.D., Hoefs, J., Simon, K., Zhang, Z.M., Li, S.G., and Hofmann, A.W., 2006, Making continental crust through slab melting: Constraints from niobium-tantalum fractionation in UHP metamorphic rutile: Geochimica et Cosmochimica Acta, v. 70, p. 4770–4782.

Xie, J.C., Yang, X.Y., Du, J.G., and Sun, W.D., 2008, Zircon U–Pb geochronology of the Mesozoic intrusive rocks in the Tongling region: implications for copper–gold mineralization: Acta Petrologica Sinica, v. 24, p. 1782–1800 (in Chinese with English abstract).

Xie, J.C., Yang, X.Y., Sun, W.D., Du, J.G., Xu, W., Wu, L.B., and Wang, K.Y., 2009, Geochronological and geochemical constrains on formation of the Tongling metal deposits, middle Yangtze metallogenic belt, east-central China: International Geology Review, v. 51, p. 388–421.

Xing, F.M., 1999, The magmatic metallogenetic belt around the Yangtze River in Anhui: Geology of Anhui, v. 9, p. 272–279 (in Chinese with English abstract).

Xing, F.M., and Xu, X., 1994, Two A-type granite belts from Anhui: Acta Petrologica Sinica, v. 10, p. 257–269 (in Chinese with English abstract).

Xing, F.M., and Xu, X., 1995, The essential features of magmatic rocks along the Yangtze River in Anhui province: Acta Petrologica Sinica, v. 11, p. 409–422 (in Chinese with English abstract).

Xiong, X.L., Adam, J., and Green, T.H., 2005, Rutile stability and rutile/melt HFSE partitioning during partial melting of hydrous basalt: Implications for TTG genesis: Chemical Geology, v. 218, p. 339–359.

Xu, Y.G., 2001, Thermo-tectonic destruction of the Archaean lithospheric keel beneath the Sino-Korean Craton in China: Evidence, timing and mechanism: Physics and Chemistry of the Earth Part a-Solid Earth and Geodesy, v. 26, p. 747–757.

Xu, Y.G., 2006, Using basalt geochemistry to constrain Mesozoic–Cenozoic evolution of the lithosphere beneath North China Craton: Earth Science Frontiers, v. 13, p. 93–104 (in Chinese with English abstract).

Yang, X.Y., and Lee, I.S., 2011, Review of the stable isotope geochemistry of Mesozoic igneous rocks and Cu–Au deposits along the Middle-Lower Yangtze metallogenic belt, China: International Geology Review, v. 53, p. 741–757.

Yang, X.Y., Yang, X.M., Zhang, Z.W., Chi, Y.Y., Yu, L.F., and Zhang, Q.M., 2011, A porphyritic copper (gold) ore-forming model for the Shaxi-Changpushan district, Lower Yangtze metallogenic belt, China: geological and geochemical constraints: International Geology Review, v. 53, p. 580–611.

Yu, L.F., Yang, X.Y., Sun, W.D., Chi, Y.Y., and Zhang, Q.M., 2008, The adakite and mineralization of the Shaxi porphyry copper–gold deposit, Central Anhui: Geology in China, v. 6, p. 1150–1161 (in Chinese with English abstract).

Yuan, F., Zhou, T.F., Fan, Y., Lu, S.M., Qian, C.C., Zhang, L.J., Duan, C., and Tang, M.H., 2008, Source, evolution and tectonic setting of Mesozoic volcanic rocks in Luzong basin: Anhui Province, Acta Petrologica Sinica, v. 24, p. 1691–1702 (in Chinese with English abstract).

Yuan, F., Zhou, T.F., Liu, J., Fan, Y., Cooke, D.R., and Jowitt, S.M., 2011, Petrogenesis of volcanic and intrusive rocks of the Zhuanqiao stage, Luzong Basin, Yangtze metallogenic belt, east China: implications for ore deposition: International Geology Review, v. 53, p. 526–541.

Yang, X.Y., Zheng, Y.F., Xiao, Y.L., Du, J.G., and Sun, W.D., 2007, Ar-40/Ar-39 dating of the Shaxi Porphyry Cu–Au deposit in the southern Tan-Lu fault zone, Anhui Province: Acta Geologica Sinica-English Edition, v. 81, p. 477–487.

Zhai, Y.S., Xiong, Y.L., Yao, S.Z., and Lin, X.D., 1996, Metallogeny of copper and iron deposits in the Eastern Yangtze Craton, east-central China: Ore Geology Reviews, v. 11, p. 229–248.

Zhai, Y.S., Yao, S.Z., and Lin, X.D., 1992, Metallogeny of iron and copper (gold) deposits in the middle-lower reaches of Yangtze River: Beijing, Geological Publishing House, p. 1–235 (in Chinese).

Zhang, B.D., Zhang, F.S., Ni, Q.S., Chen, P.R., Zai, J.P., and Shen, W.Z., 1988, Geology geochemistry and genesis discussion of quartz syenite in Anlu belt: Acta Petrologica Sinica, v. 3, p. 1–12 (in Chinese with English abstract).

Zhang, Q., Qian, Q., and Wang, Y., 2001a, An east China plateau in mid-late Yanshanian period: Implication from adakites: Science Geologica Sinica, v. 36, p. 248–255.

Zhang, Q., Wang, Y., Qian, Q., Yang, J.H., Wang, Y.L., Zhao, T.P., and Guo, G.J., 2001b, The characteristics and tectonic-metallogenic significances of the adakites in Yanshan period from eastern China: Acta Petrologica Sinica, v. 17, p. 236–244 (in Chinese with English abstract).

Zheng, Y.F., Fu, B., and Gong, B., 1995, The thermal history of the Huangmeijian intrusion in Anhui and its relation to mineralization: Isotopic evidence: Acta Geologica Sinica, v. 69, p. 337–348 (in Chinese with English abstract).

Zheng, Y.F., Fu, B., Gong, B., and Li, L., 2003, Stable isotope geochemistry of ultrahigh pressure metamorphic rocks from the Dabie-Sulu orogen in China: Implications for geodynamics and fluid regime: Earth-Science Reviews, v. 62, p. 105–161.

Zhou, B., Wang, F.Y., Sun, Y., Sun, W.D., Ding, X., Hu, Y.H., and Ling, M.X., 2008c, Geochemistry and tectonic affinity of Shahewan orogenic rapakivi from Qinling: Acta Petrologica Sinica, v. 6, p. 1261–1272 (in Chinese with English abstract).

Zhou, T.F., Fan, Y., Qian, C.C., Lu, S.M., and Cooke, D.R., 2008a, Advances on petrogenesis and metallogeny study of the mineralization belt of the middle and lower reaches of the Yangtze River area: Acta Petrologica Sinica, v. 24, p. 1665–1678 (in Chinese with English abstract).

Zhou, T.F., Fan, Y., Yuan, F., Lu, S.M., Shang, S.G., Cooke, D.R., Meffre, S., and Zhao, G.C., 2008b, Geochronology of the volcanic rocks in the Lu-Zong (Lujiang-Zongyang) basin and its significance: Science in China (Series D-Earth Sciences), v. 51, p. 1470–1482.

Zhou, X.M., and Li, W.X., 2000, Origin of Late Mesozoic igneous rocks in Southeastern China: Implications for lithosphere subduction and underplating of mafic magmas: Tectonophysics, v. 326, p. 269–287.